

# We are IntechOpen, the world's leading publisher of Open Access books Built by scientists, for scientists

6,900

Open access books available

186,000

International authors and editors

200M

Downloads

Our authors are among the

154

Countries delivered to

TOP 1%

most cited scientists

12.2%

Contributors from top 500 universities



WEB OF SCIENCE™

Selection of our books indexed in the Book Citation Index  
in Web of Science™ Core Collection (BKCI)

Interested in publishing with us?  
Contact [book.department@intechopen.com](mailto:book.department@intechopen.com)

Numbers displayed above are based on latest data collected.  
For more information visit [www.intechopen.com](http://www.intechopen.com)



---

# 3D Ultrasound Imaging in Image-Guided Intervention

---

Aaron Fenster, Jeff Bax, Hamid Neshat,  
Nirmal Kakani and Cesare Romagnoli

Additional information is available at the end of the chapter

<http://dx.doi.org/10.5772/55230>

---

## 1. Introduction

Soon after the discovery of x-rays, physicians recognized the importance of using imaging to guide interventional procedures. As imaging technology became more advanced with the development of fluoroscopic, CT, MR and ultrasound systems, image-guided interventions have become a critical tool for physicians in dealing with complex interventional and surgical procedures. Today, image-guided procedures make use of computer-based systems to provide real-time three-dimensional (3D) information of the anatomy of the patient being treated. The information is presented in various ways, such as virtual graphical image overlays, or multi-screen approaches to help the physician precisely visualize and target the anatomical site.

Since the development of Computed Tomography (CT) in the early 1970s, the availability of 3D anatomical information has revolutionized diagnostic radiology by providing physicians with 3D images of anatomical structures. The pace of development has continued with the development of 3D magnetic resonance imaging (MRI), positron Emission Tomography (PET), and multi-slice and cone beam CT imaging. These imaging modalities have stimulated the development of a wide variety of image-guided interventional procedures.

Although 2D ultrasound (2D US) imaging has been used extensively for interventional procedures, such as biopsy and guidance of ablation procedures, 3D ultrasound is slowly growing in clinical applications [1]. Today, the majority of US-based diagnostic and interventional procedures are still performed using conventional 2D imaging. Over the past two decades, university-based investigators and commercial companies have utilized both 1D and 2D arrays while developing 3D ultrasound (3D US) imaging techniques. 3D US techniques have been increasingly used in diagnosis, minimally invasive image-guided interventions and intra-operative use of imaging [2-4]. Today, most US system manufacturers provide 3D US imaging capability as part of the systems. Advances in 3D US imaging technology have resulted in high quality 3D images of complex anatomical structures and pathology, which are used in diagnosis of disease and to guide interventional and surgical procedures [5-9].

In this chapter we focus on the recent development of 3D US imaging as it applies to image-guided interventions. The chapter will briefly review how 3D US images are obtained and then will provide two examples of recent development of 3D US- guided interventional procedures.

## 2. 3D ultrasound imaging systems

### 2.1. Benefits of 3D ultrasound imaging

Conventional 2D US imaging systems making use of 1D transducer arrays allow users to manipulate the hand-held US transducer freely over the body in order to generate images of organs and pathology. While this capability is sufficient for many interventional procedures such as breast biopsy, some interventional procedures require 3D image visualization, which 3D US imaging attempts to provide. More specifically:

- Freely manipulating the conventional US transducer during the interventional procedure over the anatomy to generate 2D US images requires that users mentally integrate many 2D images to form an impression of the anatomy and pathology in 3D. In cases of interventions of complex anatomy or pathology, this approach leads to longer procedures and may result in variability in guidance of the interventional procedures.
- Since the conventional 2D US imaging transducer is held and manipulated manually, it is difficult to relocate the 2D US image at the exact location and orientation in the body at a later time. Since monitoring the progression of the interventional procedure often requires imaging of the same location (plane) of the anatomy, manual manipulation of a 2D US image is suboptimal.
- Conventional 2D US imaging does not permit viewing of planes parallel to the skin – often called C-mode. This approach is, at times, suboptimal since interventional procedures sometimes require an arbitrary selection of the image plane for optimal viewing of the pathology and guiding the interventional procedure.
- Planning the interventional procedure and therapy monitoring often require accurate lesion volume measurements. Since conventional 2D US imaging only provides a cross-section of the lesion, measurements of organ or lesion volume is variable and at times inaccurate.

The following sections review approaches used in generation of 3D US images based on 1D. An emphasis is placed on the geometric accuracy of the generated 3D images as well as the use of this technology in interventional and quantitative monitoring applications.

### 2.2. Mechanical 3D US scanning systems

Mechanical 3D US systems make use of mechanisms using motors to translate, tilt, or rotate a conventional 2D US transducer. A sequential digitized series of 2D US images and their relative positions and orientation are acquired rapidly by a computer as the 2D US transducer is moved, while the 3D US image is reconstructed. Since the scanning geometry in mechanical 3D US systems is predefined and precisely controlled by a mechanical motorized system, the relative position and orientation of the acquired 2D US images are known accurately and precisely.

These mechanical 3D scanning systems allow the user to optimize the image resolution by adjusting the angular or spatial interval between the acquired 2D image [10].

Two approaches have been used in the development of mechanical 3D US scanning systems: integrated 3D US transducers with the scanning mechanism within the transducer housing; and external mechanical fixtures that hold the housing of a conventional 2D US transducers. Both approaches have been successfully used for a variety of clinical applications including interventional applications.

### *2.2.1. Wobbling or tilting mechanical 3D US scanners*

Most US system manufacturers offer integrated 3D US transducers that are based on a mechanically-swept transducer or “wobbler”. In these systems a 1D US array is wobbled or swept back and forth inside the 3D transducer housing. Digital 2D US images that are generated while the 1D US array is wobbled, which are used in the 3D US image reconstruction. These 3D transducers are larger than conventional 2D US transducers. These types of 3D US transducers are convenient to use but require a special US machine that can control the 3D scanning and reconstruct the acquired 2D images into a 3D image.

Many interventional 3D US-guided interventional systems are currently using external fixtures for mechanical 3D scanning since researchers typically do not get access to the control of the US system for development of novel interventional systems. In this approach, a motorized custom made fixture is used to house the conventional 2D US transducer. A computer is used to control the motor to cause the US transducer to tilt or “wobble”. The video stream from the US machine is digitized using an analogue or digital frame grabber. Since the relative angle between the acquired 2D images is known, a 3D image can be reconstructed as the 2D images are acquired.

Although the external mechanical 3D scanning fixtures are bulkier than integrated 3D transducers, they can be used with any US manufacturer’s transducer, obviating the need to purchase a special 3D US machine. In addition, the external fixture approach can take advantage of improvements in the US machine (e.g., image compounding, contrast agent imaging) and flow information (e.g., Doppler imaging) without any changes in the scanning mechanism.

Both approaches used in mechanical 3D US scanning allow short imaging times, ranging from about 3 to 0.2 3D images/s. The 3D images are of high quality and also include B-mode and Doppler information.

Figure 1a is a diagram of the mechanical tilt approach of a conventional 1D array US transducer about an axis parallel to the face of the transducer, and 1b shows the tilting axis away from the face of the transducer. The latter approach is typically used in integrated 3D scanning mechanisms. In both approaches, the acquired 2D US images are arranged as a fan with an adjustable angular spacing, e.g.,  $1.0^\circ$ . To generate a 3D image, the housing of the 3D probe or external fixture remains fixed on the skin of the patient while the US transducer is wobbled. The time required to generate a 3D US image depends on the 2D US image update rate and the number of 2D images needed to generate the 3D image. The 2D US image update rate depends on the US machine settings (i.e., depth setting and number of focal zones) and number of acquired 2D US images is determined by the chosen angular separation between the acquired 2D images,

and the total scan angle needed to cover the desired anatomy. Typically, these parameters can be adjusted to optimize scanning time, image quality and the size of the volume imaged [11-16]. The most common integrated 3D transducers using the wobbling technique are used for abdominal and obstetrical imaging [17-19].

The 3D image resolution will not be isotropic. The resolution in the 3D US image will degrade in the axial direction away from the transducer due to the increasing US beam spread in the lateral and elevational directions of the acquired 2D US images. Since the acquired 2D images used to generate a 3D image are arranged as a fan, the distance between the acquired US images increases with increasing axial distance. Increasing axial distances result in decreasing spatial sampling resulting in further loss of spatial resolution in the elevational direction of the acquired 2D US images of the reconstructed 3D image [20].

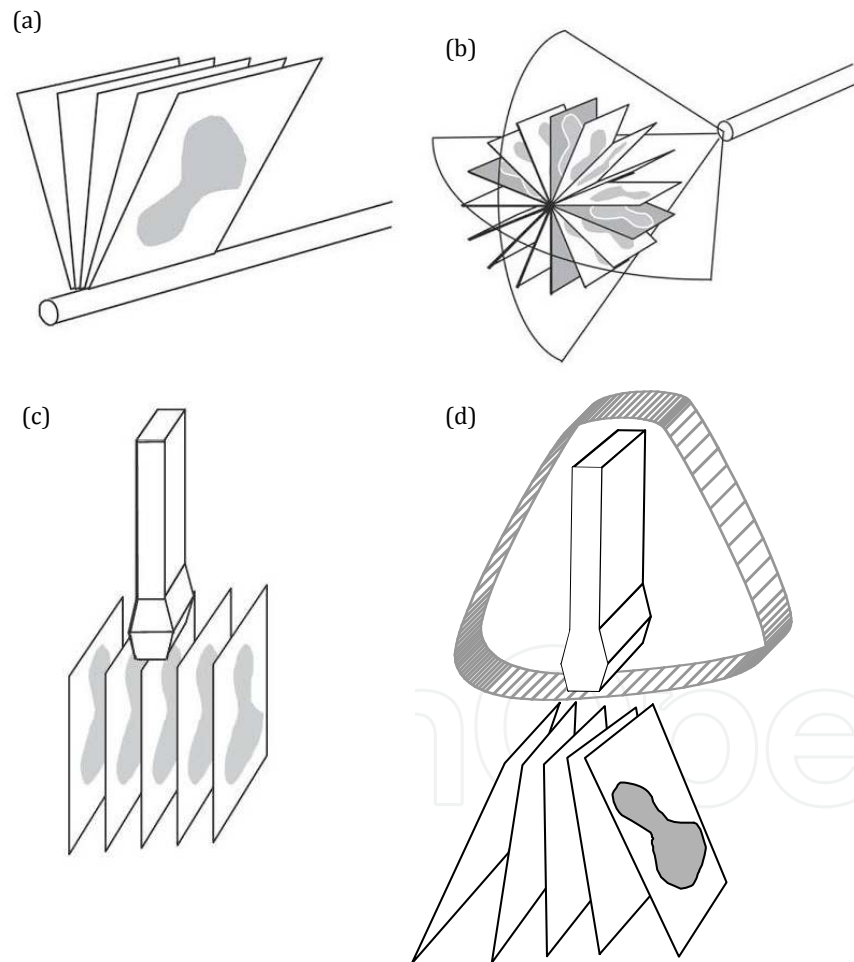


**Figure 1.** Schematic diagrams of 3D US mechanical scanning methods. (a) A side-firing TRUS transducer is mechanically rotated and the acquired images have equal angular spacing. The same approach is used in a mechanically-wobbled transducer. (b) A rotational scanning mechanism using an end-firing transducer, typically used in 3D TRUS guided prostate biopsy. The acquired images have equal angular spacing. (c) A linear mechanical scanning mechanism, in which the acquired images have equal spacing. (d) The mechanically tilting mechanism, but integrated into a 3D US transducer. The US transducer is “wobbled” inside the housing of the transducer.

### 2.2.2. Linear mechanical 3D scanners

Linear scanners mechanisms use an external motorized fixture to move the conventional 2D transducer across the skin of the patient. The 2D transducer can be fixed to be perpendicular to the surface of the skin or at an angle for acquiring Doppler images. The spacing between the acquired 2D images is adjustable but constant during the scan so that the acquired 2D images are parallel and uniformly spaced (see Fig. 1c). The velocity of the transducer as it is being scanned is adjusted to obtain 2D images with an appropriate spatial interval for generating high quality 3D images [10].

The predefined spacing between the acquired 2D US images allows 3D images to be reconstructed while the 2D US images are being acquired. In the direction parallel to the acquired 2D US images the resolution of the reconstructed 3D US image will be the same as the original 2D US images. However, in the direction of the 3D scanning, the resolution of the reconstructed 3D image will be equal (if spatial sampling is appropriate) to the elevational resolution of the acquired 2D US images. Thus, the resolution of the 3D US image will be poorest in the 3D scanning direction due to greater spread of the US beam in the elevational direction [21].

This scanning approach is not typically used in interventional applications; however, it has been successfully implemented in many vascular B-mode and Doppler imaging applications, particularly of for carotid arteries [11, 22-30] and tumor vascularization [25, 31-33].

### 2.2.3. Endo-cavity rotational 3D scanners

The endo-cavity rotational 3D scanning approach has been used extensively in 3D US-guided prostate interventional procedures. In this approach an external fixture or internal mechanism is used to rotate an endo-cavity transducer (*e.g.*, a transrectal ultrasound (TRUS) probe, see Fig. 1b) about its long axis. Endo-cavity transducers using an end-firing approach are typically used for prostate biopsy. When these types of conventional transducers are rotated by the motorized fixture, the set of acquired 2D images will be arranged as a fan (Fig. 1b), intersecting in the center of the 3D US image, resulting in an image as shown in Fig. 2. To obtain a 3D image of the prostate as in Fig. 2, an end-firing transducer is typically rotated by 180° [16].

Endo-cavity transducers using a side-firing 1D array are typically used in prostate brachytherapy, cryotherapy and focal therapy. When using these types of conventional transducers, the acquired images will also be arranged as a fan, but intersect at the axis of rotation of the transducer (see Fig. 1a). The side-firing transducer is typically rotated from 80° to 110° to obtain a 3D TRUS image of the prostate [16, 34, 35]. Figure 2 shows that endo-cavity scanning transducer used to image the prostate for 3D US-guided therapy [6, 9, 11, 25, 34, 36-39]

For scanning systems used for 3D US-guided prostate biopsy, the end-firing transducer is rotated by at least 180° about a fixed axis that perpendicularly bisects the transducer array. In this approach, the resolution of the 3D image will not be isotropic. Since the spatial sampling is highest near the rotation axis of the transducer and the poorest away from the axis of rotation of the transducer, thus the resolution of the 3D US image will degrade as the distance from the rotational axis of the transducer is increased. In addition, the axial and elevational resolution will decrease as the distance from the transducer is increased, as discussed above. The

combination of these effects will result in a 3D US image resolution that is best near the transducer and the rotational axis, while being poorest away from the transducer and rotational axis.

3D rotational scanning with an end-firing transducer is most sensitive to the motion of the transducer and patient since the axis of rotation is in the center of the 3D US image. Any motion during the 3D scan will cause a mismatch in the acquired 2D US images, resulting in artifacts in the center of the 3D US image. Artifacts in the center of the 3D US image will also occur if the axis of rotation is not accurately known; however, proper calibrations can remove this source of potential error. Thus, for interventional applications such as 3D US-guided prostate biopsy or brachytherapy, the rotational scanning mechanism is typically supported by a stabilization apparatus [16, 34, 40].

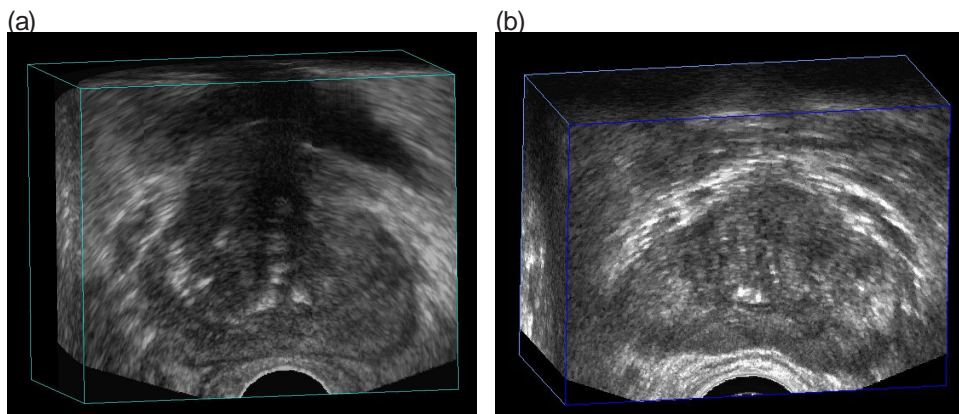


**Figure 2.** The 3D US of the prostate displayed using the multi-planar reformatting approach: (a) An end-firing TRUS prostate cube-view 3D image, allowing the sides to be translated and angles to reveal the desired anatomy. (b) A 3D TRUS image acquired using a side-firing transducer using the mechanical rotation approach.

#### 2.2.4. Free-hand scanning with position sensing

Some 3D US-guided interventional procedures are making use of 3D scanning techniques that do not require a mechanical scanning device. In this approach, the user holds and manipulates a conventional US transducer to cover the patient's anatomy being investigated. Since construction of a 3D US image requires that the position and orientation of the conventional transducer be known, free-hand scanning requires a method to track the positions and orientations of the transducer as it is being moved. All methods to accomplish this task require a sensor to be mounted on the transducer to allow measurement of the conventional 2D transducer's position and orientation as it is moved over the body.

Over the past 2 decades, several approaches for free-hand scanning have been developed: tracked 3D US with articulated arms, free-hand 3D US with acoustic sensing, free-hand 3D US with magnetic field sensing, and image-based sensing (speckle decorrelation). The method used most commonly is the magnetic field sensing approach with several companies providing

the sensing technology: Ascension – Bird sensor [3] Polhemus – Fastrack sensor [41] and Northern Digital – Aurora sensor [4].

The most successful free-hand 3D US scanning approach used in interventional procedures makes use of magnetic field sensors, as well as applications such as echocardiography, obstetrics, and vascular imaging [3, 4, 41-51]. To track the transducer during generation of a 3D US image, a small receiver is mounted on the transducer containing three orthogonal coils allowing six-degrees-of-freedom sensing. The small receiver mounted on the transducer measures the strength of the magnetic field in three orthogonal directions, which is generated by a time-varying 3D magnetic field transmitter placed near the patient. The position and orientation of the transducer is calculated by continuously measuring the strength of the three components of the local magnetic field.

Since magnetic field sensors are small and unobtrusive devices, they allow the transducer to be tracked without the need for bulky mechanical devices, and without the need to keep a clear line of sight as required by optical tracking methods. Since magnetic field sensors are sensitive to electromagnetic interference or ferrous (or highly conductive) metals located nearby, geometric tracking errors can occur leading to distortions in the 3D US image. Thus, metal beds used in procedures, or surgical rooms can cause significant distortions. However, modern magnetic field sensors have been produced to be less susceptible to these sources of error, particularly ones that use a magnetic transmitter placed between the bed and the patient.

### **3. 3D Ultrasound-guided focal liver ablation**

#### **3.1. Clinical problem**

Hepatocellular carcinoma (HCC) is the fifth most common diagnosed malignancy and the third most frequent cause of cancer related deaths worldwide [52]. Incidence is particularly high in Asia and sub-Saharan Africa due to the large incidence of hepatitis B and C, both of which are complicated by hepatic cirrhosis, which is the greatest risk factor for HCC. Recently, increasing trends in HCC have been reported from several Western countries [53]. Furthermore, the liver is the second most common site of metastatic cancer arising in other organs.

When feasible, surgical resection or liver transplant is the accepted standard therapeutic approach, and currently has the highest success rate of all treatment methods for primary and metastatic liver cancer. Unfortunately, only 15% of patients are candidates for surgery [54, 55]. Patients who do not qualify for surgery usually are offered other therapeutic solutions such as chemotherapy and radiotherapy, but unfortunately have variable limited success rates.

Minimally invasive percutaneous techniques, such as radio-frequency (RF) and microwave (MW) ablation of malignant tissue in the liver is a rapidly expanding research field and treatment tool for those patients who are not candidates for surgical resection or transplant. In some cases this acts as a bridge to liver transplantation [54, 56]. Due to low complications rates and shorter recovery times, the indications for these minimally invasive procedures are constantly increasing. However, these methods have a higher local recurrence rate than surgical resection, mostly due to insufficient or inaccurate local ablation of cancerous cells [56, 57].

Microwave energy-induced tissue heating by near-field probes is emerging as a common thermal treatment of liver tumors [58]. Application of MW for tumor ablation has multiple advantages over other techniques, including higher treatment temperatures and the ability to create larger uniformly shaped ablation zones in shorter time periods. However, the accurate placement of the probe is critical in achieving the predicted treatment goal [59]. The current standard of care uses CT images for planning and 2D US image guidance for intra-operative guidance of the ablation probe(s) into the target lesion. However, this approach suffers from several disadvantages, such as: (1) 2D US imaging requires physicians to mentally integrate many 2D images to form an impression of the anatomy and pathology, leading to more variability in guidance during interventional procedures; (2) 2D US does not permit the viewing of planes parallel to the skin, (3) liver deformation and motion artifact due to breathing reduces targeting accuracy, (4) 2D US-based for measurement of tumor volume needed for the treatment plan is variable and at times inaccurate, and (5) the detection and tracking of the needle delivering the thermal energy in the liver is crucial for accurate placement of the needle relative to the tumor, but can be difficult using 2D US. 3D US imaging of the liver and target may help to overcome these disadvantages resulting in improved accuracy of probe placement and improved ablation of the lesion.

The use of 3D US-guidance for focal liver tumor ablation is based on the fact that the use of 3D US will show the features of liver masses and the hepatic vasculature more clearly, allow guidance of the ablation probes to the target more accurately, and allow more accurate monitoring of the ablation zone during the procedure and at follow up.

### **3.2. 3D US Scanner for focal liver tumor ablation**

We have developed 3D US guidance systems for improving cancer diagnosis and treatment by introducing hardware and software innovations [21, 60-64]. Our previous efforts have been extended to the development of a 3D US-guidance system for treating HCC. Specialized hardware and software tools are used that allow 3D acquisition of 3D US images, real-time registration of the pre-operative CT to intra-operative 3D US images, and tracking of the ablation probes during insertion into the target. This is accomplished by registering previously acquired contrast CT images that show the location of the target lesion to near real-time 3D US images, plus providing visualization and guidance tools to guide the procedure.

The 3D US scanning system consists of: a hand-held electro-mechanical motor/encoder assembly to move a conventional 2D US imaging transducer in a fan shaped, linear or hybrid motion to a maximum angular limit of 60 degrees and/or 30 mm linear extent to acquire a series of 2D US images; and, a PC equipped with a digital frame grabber and software components to control the motor assembly, acquire 2D images, reconstruct them in 3D, and visualize them in 3D.

#### *3.2.1. Mechanical design*

The handheld 3D scanning device is motorized and constructed with two mechanical systems for generating a linear and tilt scanning motions of the transducer is shown schematically and photographically in Figs. 3 and 4. The linear scanning system is operated with a geared DC motor and lead screw providing linear translation. The tilt motion is generated via a paral-

logram linkage, which is mounted on the carriage of the linear slide. A second geared DC motor is used to generate the tilt motion, allowing for independent control of the two systems.

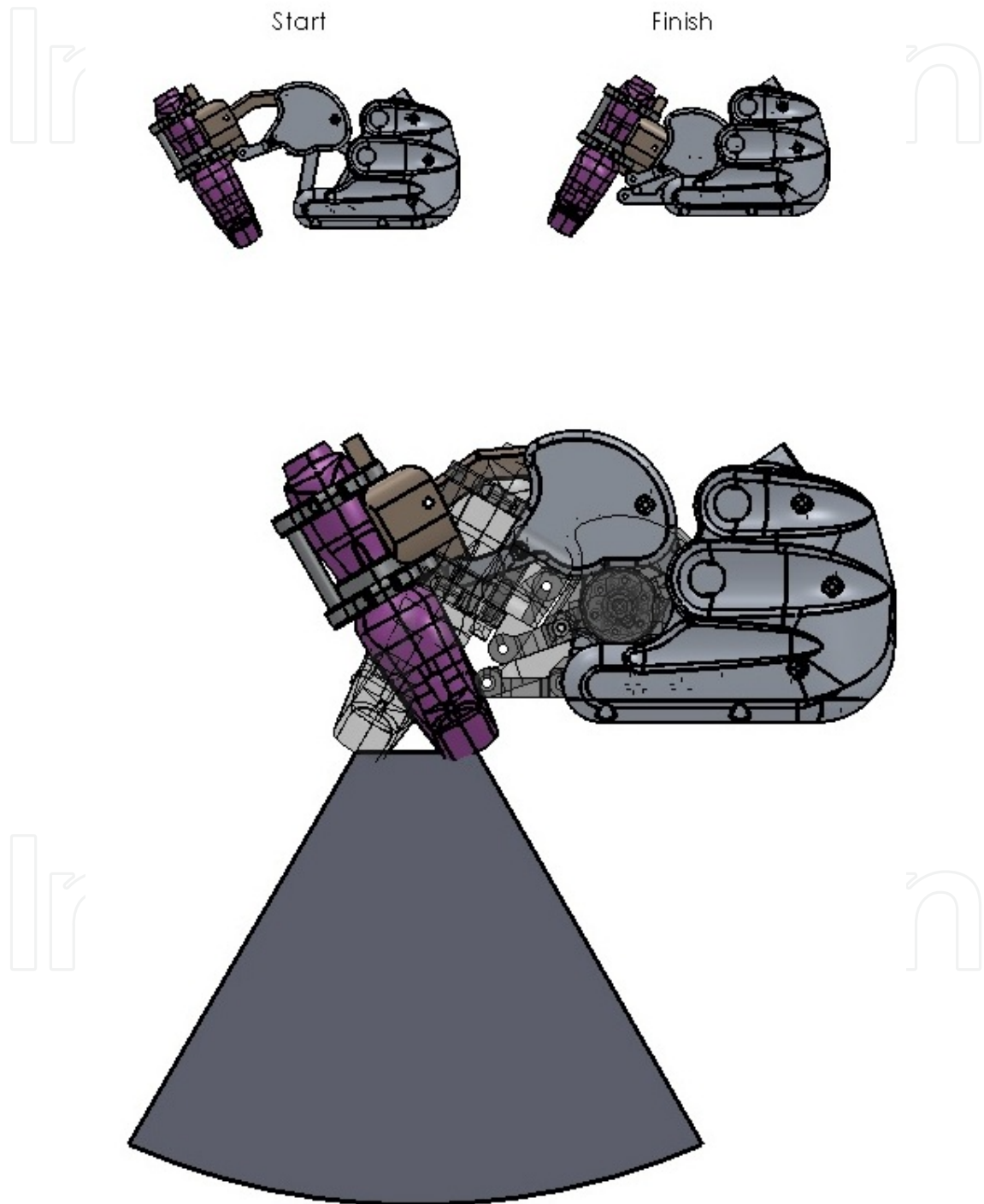


**Figure 3.** Schematic diagram of the hybrid 3D US scanner for used in the focal liver ablation procedure. The diagram shows the start and end positions of the hybrid (linear and tilt) scan.

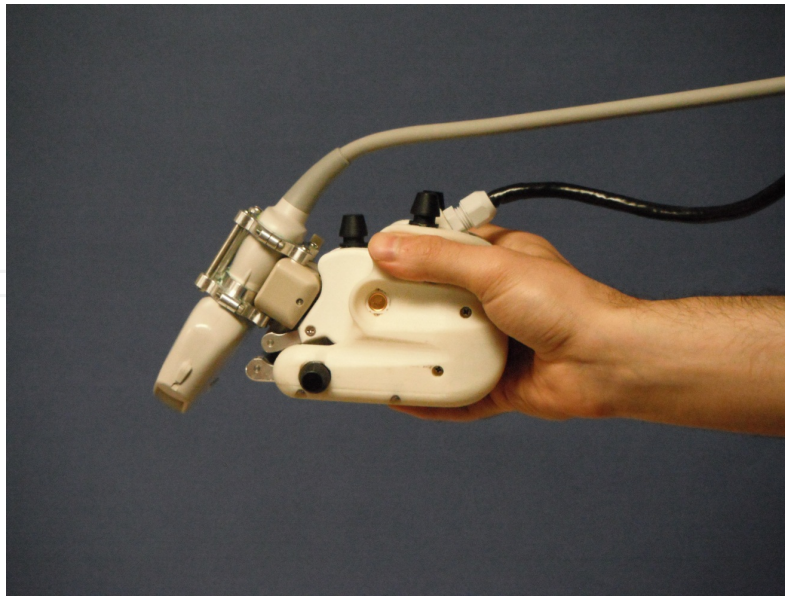


**Figure 4.** Photograph of hybrid scanner with abdominal ultrasound transducer mounted and ready for scanning.

The 3D scanning device has three modes of operation: a linear translation, in which the transducer (oriented perpendicular to the surface or at an angle for Doppler imaging) is translated along a straight line parallel to the patient's surface. This motion generates a rectangular volume shown in Fig. 5a. The second mode generates a tilt motion (or wobbling), in which the transducer is rotated about its face resting on the patient's skin surface (Fig. 5b). The third mode is a combination of the first two modes that creates a combined (or hybrid) motion. The transducer is rotated as it is moved along a surface covering a larger volume than either of the first two modes (Fig. 5c). For example, if transducer with linear array is used at 15cm depth setting on the ultrasound machine (typical depth for abdominal imaging), hybrid scanning gives a volume that is three times larger than the linear mode and 47% larger than the tilt mode only.

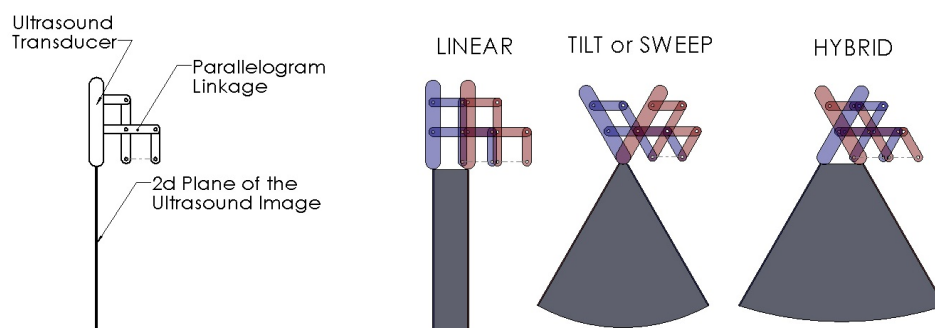


**Figure 5.** Schematic diagrams showing the three modes of operation of the mechanical compound 3D US scanning device. On the left is the schematic of the linkage and the right are the linear, tilt and hybrid motions.

The 3D scanning system parameters can be set by the user: *Scanning mode*: Three different modes of linear, tilt and combined (or hybrid, a combination of both linear and tilt imaging modes to maximize the field-of-view) are available depending on the anatomy of body parts being scanned and the image requirements. *Scan Extent*: Maximum extent of linear translation (typically 2.5 cm) or tilt angle (typically 60 deg) can be set individually to the extremes values. *Scan Spacing*: Elevational linear and angular spacing can be set to optimize the trade-off between the scanning time and the scan spacing. *Frame-Rate*: The rate at which images are digitized by the frame grabber is set (typically 15 frames/s). *Scanning Depth*: Maximum scanning depth can be set prior to each scan for accurate reconstruction of the volumes.

### 3.2.2. Validation methods

Since the hybrid scanning mode involves coordination between two acquisition methods, it was tested in terms of accuracy of 3D image generation. We used two custom made phantoms with known geometry. The validation experiments were performed using the handheld 3D US scanning device in hybrid scanning mode using a two-dimensional conventional curved array ultrasound transducer used for abdominal applications (Toshiba, PVT-375BT).

*Geometrical Error in 3D reconstruction*: This test was designed to measure the accuracy of the 3D reconstruction of the 3D hybrid scanner in three directions. The test phantom was made of a grid of known dimensions made with 0.1 mm thick nylon monofilament threads wrapped around an accurately machined frame to form a 4-layer grid. Each layer was slightly shifted from the layer above to avoid acoustic shadowing. The distance between any two layers was 1cm. The phantom was submerged in a 15% glycerol solution [61] and imaged at different depth settings. The acquired 3D US images were then viewed and analyzed by measuring the distances between the images of the monofilaments and comparing them to the expected values.

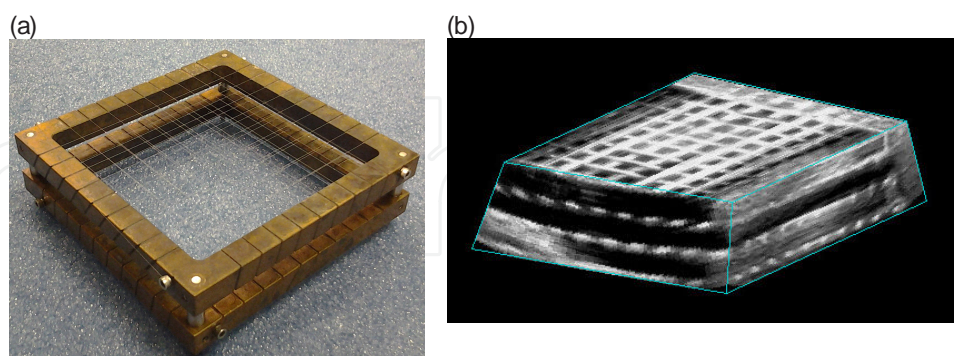


**Figure 6.** (a) Photograph of the 3D monofilament thread grid, which was used to validate the 3D reconstruction of the ultrasound image. (b) The 3D ultrasound image of the phantom, showing the grid of threads.

*Error in 3D volume measurements*: In the second test, we assessed the accuracy in measuring volumes using our system. For this experiment, several spherical phantoms with different sizes were made of tissue mimicking agar [65]. The volume of each of these spherical phantoms was measured prior to embedding them in a cube of tissue mimicking agar phantom. The spherical

phantoms were then imaged with our hybrid scanner, viewed in the 3D visualization software, and manually segmented. The volume of spherical structures were calculated and compared with the expected values.

### 3.2.3. Validation results

Testing the 3D hybrid scanner with the 3D thread phantom showed that mean error in the measured values of the distances in the X, Y and Z directions were 3.6%, 2.5% and 5.7% respectively. A one-sample t-test was performed to compare the measured distance values with the known distance value of 1cm, showed there was no statistical significant difference between the measured values and expected values between the threads.

Validation of volume measurements using the hybrid scanner were carried out by imaging a tissue mimicking agar sphere with a volume of 10 cm<sup>3</sup> embedded in a block of tissue mimicking agar phantom. The measurements were performed at two different depth settings on the ultrasound machine (10 and 15 cm). The mean errors of the volume measurement were 5.7% and 4.4% for the 10cm and 15cm depth settings respectively, demonstrating that the hybrid scanner can be used to make sufficiently accurate volumetric measurements.

*In-vivo experiments:* After obtaining institutional research board (IRB) approvals, we investigated the use of the scanner in thermal ablation treatment of primary hepatic tumors. Figure 7 shows a 3D US image acquired during the microwave ablation procedure of a primary (hepatocellular) tumor. It shows application of the hybrid mode in acquiring volumes large enough to include both the ablated tumor region as well as all ablation needles in two different views.

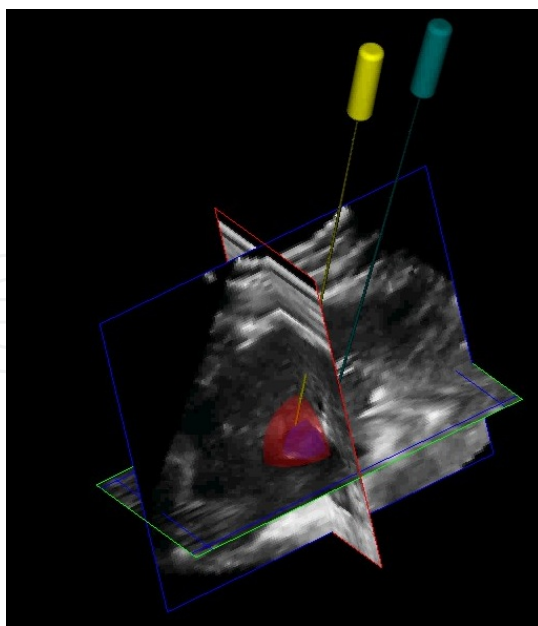


**Figure 7.** 3D ultrasound image of a primary (hepatocellular) tumor with two microwave applicators in place. The applicators and tumor have been segmented and displayed in 3D allowing the interventional radiologist to examine the placement accuracy of the applicators in the tumor. In addition, the ablation zone has also been superimposed.

## 4. 3D ultrasound guided prostate biopsy

### 4.1. The clinical problem

Prostate Cancer (PCa) is the most commonly diagnosed malignancy in men, and is found at autopsy in 30% of men at age 50, 40% at age 60, and almost 90% at age 90 [66, 67]. Worldwide, it is the second leading cause of death due to cancer in men, accounting for between 2.1% and 15.2% of all cancer deaths [68, 69]. Symptoms PCa are generally absent until extensive local growth or metastases develop. When diagnosed at an early stage, the disease is curable [70, 71], and even at later stages treatment can be effective [72]; however, once the tumor has extended beyond the prostate, the risk of metastases and locally aggressive cancer increases. Clearly, early diagnosis, accurate staging of prostate cancer, and appropriate therapies are critical to the patient's well-being.

In managing patients with possible PCa, the challenges facing physicians are to: (a) diagnose clinically relevant cancers at a curable stage; (b) stage the disease accurately; (c) apply appropriate therapy accurately to optimize destruction of cancer cells while preserving normal tissues and function; and (d) follow patients to assess side effects and therapy effectiveness. This section focuses on improving early PCa diagnosis and staging with the use of 3D ultrasound-guided prostate biopsy.

Since not all cancers are palpable by digital rectal exam (DRE), PCa diagnosis is established by histological examination of prostate tissue obtained most commonly by trans-rectal ultrasound (TRUS)-guided biopsy. Prostate needle biopsy is the only definitive diagnostic modality capable of confirming malignancy, and is now always performed with TRUS guidance.

Since many small tumors are not detected by TRUS or DRE, biopsy samples are obtained from predetermined regions of the prostate known to have a high probability of harboring cancer. These are typically in the peripheral zone (PZ), which harbors 80% of all PCs and a higher proportion of clinically significant ones, and close to the capsule, as most cancers are thought to start within 5mm of the prostate capsule. Most centers are now taking 8-12 cores or more as part of their routine assessment [73-76].

TRUS biopsies are now performed with a thin, 18-gauge needle mounted on a spring-loaded gun connected to the TRUS probe, forcing the needle to stay in the imaging plane. Each core is separately identified as to the prostate region from which it was drawn, so that the pathologist can report the extent and grade of the cancer within each region.

Since prostate volume sampled by the biopsy is small, and PCa is often multi-focal, involving only a small volume of the prostate in the early stages of the disease [77, 78], the probability for obtaining a sample of the tumour on biopsy is small. Thus, a negative biopsy may be, in fact, false, and the patient may be harbouring cancer at an early and curable stage. Various reports have shown that the false negative rate ranges from 10% to 25% [73, 74]. Since cancer is still present in 1/10 to 1/4 of patients with a negative first biopsy, the current biopsy procedure is still suboptimal [74, 79]. Clearly, an improved procedure with improved planning and recording of biopsy locations is necessary to resolve these issues.

Due to the increasing number of younger men with early and potentially curable PCa undergoing repeated prostate biopsy, it is therefore vital not to re-biopsy the same area if the original biopsy was negative, and it is particularly vital to re-biopsy the same area if a possible abnormal area was detected on first biopsy as ASAP [80]. Thus, the locations of the cores obtained from the prostate must be known accurately to help guide the physician during the repeat biopsy [81, 82], to help in correlating any imaging evidence of the disease, and to provide improved planning for subsequent therapy.

#### **4.2. Multi-modality directed prostate biopsy**

A variety of imaging techniques and molecular imaging probes are being investigated to improve early detection of PCa. Different magnetic resonance imaging (MRI) techniques have been evaluated using body and endo-rectal coils, contrast enhancement, and different pulse sequences [83-85] resulting in disease detection sensitivity and specificity of 80-88% and 75-95%, respectively [84, 86, 87]. Positron emission tomography (PET) (combined with CT or MRI) is used to detect early disease, with the newer PET imaging probes proving to be the more promising [88-90]. Although progress has been made with improved PET and MRI techniques, they do not yet have ideal specificity or sufficient accuracy to assess the grade of the cancer; thus a biopsy of suspicious lesions on MRI or PET is required to provide a definitive diagnosis and grade of the disease. Systems have been developed to perform biopsies in the MRI suite; however, the cost of the equipment and prolonged use of the MRI is extremely expensive and likely prohibitive given the large number of patients requiring biopsy. Unfortunately, conventional 2D TRUS guidance of the biopsy procedure limits the physician's ability to target locations identified as suspicious on other modalities.

As we currently do not have a highly sensitive and specific imaging test for local staging of PCa, there is a growing belief that the optimal method to guide prostate biopsy will involve not just one, but a combination of imaging modalities. 3D TRUS imaging combined with functional or molecular imaging from another imaging modality such as radiopharmaceutical imaging (PET, SPECT), or magnetic resonance imaging (MRS, MRI) may provide the best approach for guiding prostate biopsy.

#### **4.3. 3D TRUS-guided prostate biopsy system**

Since ultrasound imaging is the clinical standard for image-guided biopsy of the prostate, we have developed a 3D TRUS-based navigation system that provides a reproducible record of the 3D locations of the biopsy targets throughout the procedure and allows fusion with MR images with identified lesions for targeting.

The system we have developed is a mechanical 3D biopsy system that maintains the procedural workflow, minimizing costs and physician retraining. This mechanical system has 4 degrees-of-freedom (DOF) and has an adaptable cradle that supports commercially available end-firing TRUS transducers used for prostate biopsy [16]. It also allows real time tracking and recording of the 3D position and orientation of the biopsy needle as the physician manipulates the TRUS transducer. The following describes the components of the system, including hardware,

modeling and segmentation algorithms, and system validation using a multi-modal US/CT prostate phantom.

Our approach involves the use of a device composed of two mechanisms shown as a schematic in Figure 8. The system is composed of an articulated multi-jointed stabilizer and a transducer tracking mechanism.



**Figure 8.** A schematic diagram of the mechanical tracker, which supports the TRUS transducer and attached cradle. This configuration constrains the TRUS probe motion to three degrees-of-freedom and one degree of translation along the axis of the probe. The system is mounted at the base of a stabilizer while the linkage allows the TRUS transducer to be manually manipulated about a remote center of motion (RCM), which is at the center of the ultrasound transducer tip.

The end-firing TRUS transducer with the biopsy needle guide in place is mounted to the mechanical tracking mechanism in a manner where the US probe is free to rotate around its longitudinal axis (Fig. 8). The tracking assembly is attached to a stabilizer, which is mounted on a free-standing cart. Thus, the physician can manipulate the tracking mechanism freely, insert the transducer through the anus, and rotate the transducer in order to acquire a 3D image of the prostate. The tracking linkage contains angle-sensing encoders mounted to each joint in order to transmit to the computer the angles between the arms. This arrangement allows the computer to determine the relative position of the transducer as it is being manipulated. Since the biopsy gun is mounted onto the transducer and its position relative to the transducer is calibrated, the needle location can be calculated.

The mechanical tracking device is a spherical linkage assembly, in which the axis of the joints converge to a common point on the remote center of motion (RCM). The RCM design minimizes targeting errors within the prostate. As the TRUS transducer is constrained through a stationary point, the physician's movements are replicated at a scaled down rate (minified through the RCM), minimizing changes in morphology and dislocation of the prostate. In addition, the RCM enables a precision equivalent to that of robotic assisted machines. Thus,

the system improves the physician's ability to accurately biopsy a point of interest within the patient's prostate.

#### 4.4. Prostate biopsy procedure

To perform a 3D US-guided prostate biopsy, the end-firing US transducer is mounted onto the tracking assembly such that the tip of the probe is initially set to the RCM point of the tracker linkage. The physician inserts the TRUS transducer into the patient's rectum and aligns the prostate to the center of the 2D TRUS image. A 3D image of the prostate is then acquired by rotating the transducer 180 degrees about its longitudinal axis (Fig. 1b) [91]. A graphical model of the prostate is then generated by a semi-automatic 3D segmentation algorithm [61, 92-94]. After the prostate model has been constructed, the physician can then manipulate the 3D image on the computer screen and select locations to biopsy. After all of the biopsy targets have been selected, the system then displays the 3D needle guidance interface (Fig. 9), which facilitates the systematic targeting of each biopsy location previously selected. Other images or information (*e.g.*, MRI or PET/CT images), if available, are registered to the 3D TRUS image and displayed as an overlay on the computer screen (Fig. 10).

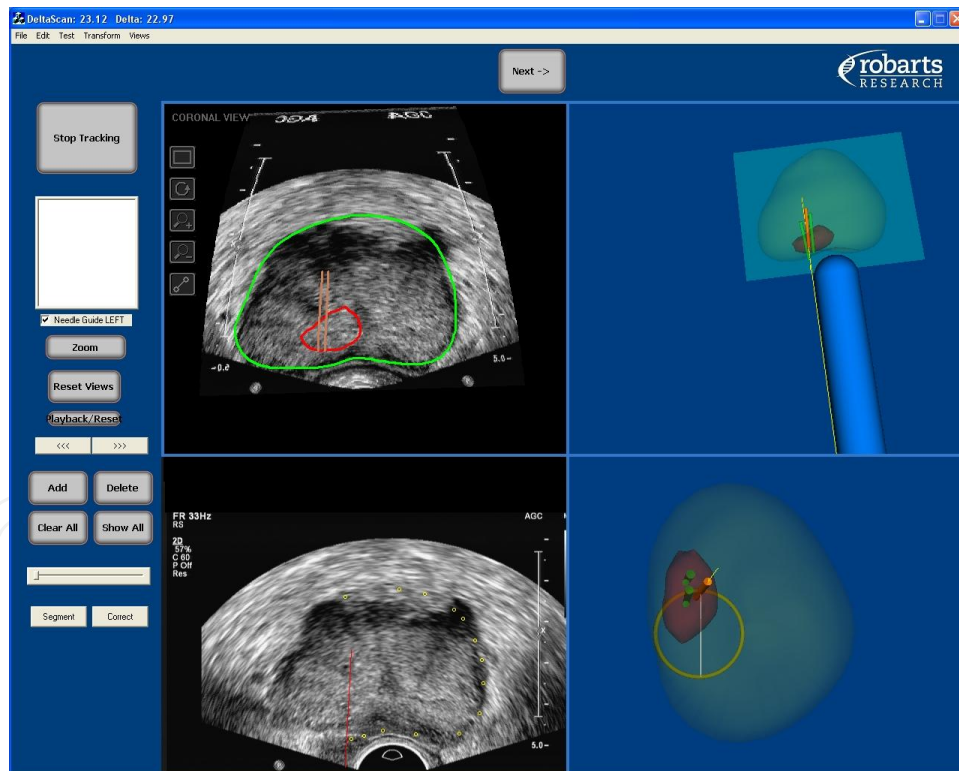


**Figure 9.** The 3D US-guided prostate biopsy system interface is composed of 4 windows: (top left) the 3D TRUS image dynamically sliced to match the real-time TRUS probe 3D orientation, (bottom left) the live 2D TRUS video stream, (right side) and the 3D location of the biopsy core is displayed within the 3D prostate models. The targeting ring in the bottom right window shows all the possible needle paths that intersect the preplanned target by rotating the TRUS about its long axis. This allows the physician to move the TRUS probe to the target (highlighted by the red dot) in the shortest possible distance. The segmented tumor to be targeted is outlined and rendered in red.

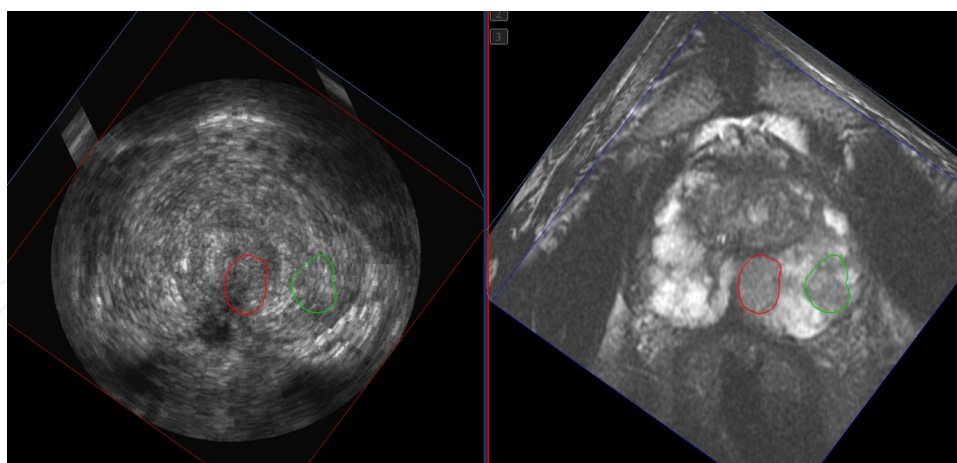


**Figure 10.** Registered 3D TRUS and MRI images of the same patient showing delineated suspicious lesions identified in the MR images (right panel). The MR images were then registered with the 3D TRUS images (left panel) and the delineated two regions (red and green) superimposed on the 3D TRUS images. These regions were then targeted with the 3D TRUS-guided biopsy system shown in Figs. 8 and 9.

As the physician manually manipulates the TRUS transducer, the 3D location and orientation of the transducer and needle trajectory are tracked in real-time throughout the procedure on the computer screen. Figure 9 illustrates the biopsy interface, which is composed of 4 windows: the live 2D TRUS video stream, the 3D TRUS image, and two 3D model views. The 2D TRUS window displays the real-time 2D TRUS image from the US machine. The 3D TRUS window contains a 2D slice of the 3D static model in real-time to reflect the expected orientation and position of the TRUS probe. This correspondence allows the physician to compare the 3D image with the real-time 2D image to determine if the prostate has moved or deformed to a prohibitive extent. After each biopsy, the biopsy location is recorded in 3D from the tracker orientation, and the system is ready for the next biopsy. After the needle is withdrawn, a 3D image may be obtained to determine if there is any movement or swelling of the prostate.

#### 4.5. Clinical evaluation of 3D TRUS/MRI-guided biopsy

Clinical studies are being performed at a number of centers to evaluate the clinical impact of fusion of MRI to intra-biopsy 3D TRUS for 3D US-guided targeted biopsy of suspicious MRI lesions on prostate cancer detection and grading. At the London Health Sciences Centre in London, Canada, prostate MR imaging was performed on 31 patients with clinical suspicion for prostate cancer in advance of their 3D TRUS-guided biopsy. T2, diffusion-weighted and dynamic-contrast enhanced MR sequences were collected in a 3T MRI system with an endorectal RF coil. All suspicious lesions in the MR images were then identified and delineated on the images, which were then registered to the 3D TRUS image obtained during the biopsy procedure (see Figure 10). Using the 3D TRUS-guided biopsy system, prostate biopsy cores were targeted toward each suspicious delineated MRI lesion, which were displayed on the 3D TRUS image. A standard 12-core set of random biopsies was also performed on each patient and used as an internal control.

The results of this study showed that MRI-3D TRUS fusion was successfully performed and the targeted biopsy needle cores had a significantly higher rates of prostate malignancy (30.0%) compared to random, sextant cores (10.0%). In total, prostate cancer was biopsy confirmed in 11 patients; however, only 7 of these patients had abnormal MRI findings (even in retrospective analysis) and were sampled with targeted MRI-3D TRUS fusion. Random sampling detected the remaining four patients. A significantly higher percentage of the targeted biopsy cores (47+/-26%) contained cancer compared to the randomly sampled cores (28+/-26%), and for 3 patients, the MRI-targeted cores detected a higher Gleason cancer grade than the random cores, modifying potential treatment modalities. This study showed that MRI-3D TRUS fusion allows for superior sampling of prostate cancer visible on MRI. This technology may benefit both cancer detection and accurate malignancy grading for appropriate therapeutic management; however, further testing is needed to establish the full utility of this technology.

## 5. Conclusions

Clinical evaluation of the mechanical tracking systems for use in 3D ultrasound guidance for focal liver ablation and prostate biopsy have been found to be easy to use. The tracker permits manual motions identical to the current conventional procedure, where restricted movements are produced by the US probe in the patient's rectum.

Reconstruction of 3D TRUS images using the hybrid approach for focal liver ablation, and rotational approach for prostate biopsy can produce accurate 3D images without significant visible discontinuity or artefacts. Volume calculations from the 3D TRUS image have shown that the 3D US systems can generate accurate volume measurements.

The patient studies have demonstrated that it is possible to minimize the effects of liver and prostate motion through a variety of mechanical and software mechanisms. However, improved solutions, which correct any patient motion automatically are still needed. It is not possible to control all patient/organ motion during the procedures, particularly if the patient moves during the prostate biopsy procedure after the firing of the prostate biopsy needle. To overcome this problem, a software module would have to be developed to inform the physician that the prostate has moved and then correct for the motion and deformation. This task must be done quickly, possibly in real-time, using an implementation of the software in a graphical processing unit (GPU).

## Acknowledgements

The authors gratefully acknowledge the financial support of the Canadian Institutes of Health Research, the Ontario Institute for Cancer Research, the Ontario Research Fund, the National Science and Engineering Research Council, and the Canada Research Chair program.

## Author details

Aaron Fenster<sup>1,2,3</sup>, Jeff Bax<sup>1,2</sup>, Hamid Neshat<sup>1,2</sup>, Nirmal Kakani<sup>3</sup> and Cesare Romagnoli<sup>3</sup>

1 Robarts Research Institute, University of Western Ontario, London, Canada

2 Biomedical Engineering Department, University of Western Ontario, London, Canada

3 Department of Medical Imaging, University of Western Ontario, London, Canada

## References

- [1] Elliott ST. Volume ultrasound: the next big thing? *Br J Radiol.* 2008;81(961):8-9.
- [2] Downey DB, Fenster A, Williams JC. Clinical utility of three-dimensional US. *Radiographics.* 2000;20(2):559-71.
- [3] Boctor EM, Choti MA, Burdette EC, Webster Iii RJ. Three-dimensional ultrasound-guided robotic needle placement: an experimental evaluation. *Int J Med Robot.* 2008;4(2):180-91.
- [4] Hummel J, Figl M, Bax M, Bergmann H, Birkfellner W. 2D/3D registration of endoscopic ultrasound to CT volume data. *Phys Med Biol.* 2008;53(16):4303-16.
- [5] Carson PL, Fenster A. Anniversary paper: evolution of ultrasound physics and the role of medical physicists and the AAPM and its journal in that evolution. *Med Phys.* 2009;36(2):411-28.
- [6] Wei Z, Wan G, Gardi L, Mills G, Downey D, Fenster A. Robot-assisted 3D-TRUS guided prostate brachytherapy: system integration and validation. *Med Phys.* 2004;31(3):539-48.
- [7] Smith WL, Surry K, Mills G, Downey D, Fenster A. Three-dimensional ultrasound-guided core needle breast biopsy. *Ultrasound in Med and Bio.* 2001;27(8):1025-34.
- [8] Chin JL, Downey DB, Onik G, Fenster A. Three-dimensional prostate ultrasound and its application to cryosurgery. *Tech Urol.* 1996;2(4):187-93.
- [9] Chin JL, Downey DB, Mulligan M, Fenster A. Three-dimensional transrectal ultrasound guided cryoablation for localized prostate cancer in nonsurgical candidates: a feasibility study and report of early results. *J Urol.* 1998;159(3):910-4.
- [10] Smith WL, Fenster A. Optimum Scan Spacing for Three-Dimensional Ultrasound by Speckle Statistics. *Ultrasound in Medicine and Biology.* 2000;26(4):551-62.
- [11] Fenster A, Tong S, Sherebrin S, Downey DB, Rankin RN. Three-dimensional ultrasound imaging. *SPIE Physics of Medical Imaging.* 1995;2432:176-84.

- [12] Delabays A, Pandian NG, Cao QL, Sugeng L, Marx G, Ludomirski A, et al. Trans-thoracic real-time three-dimensional echocardiography using a fan-like scanning approach for data acquisition: methods, strengths, problems, and initial clinical experience. *Echocardiography*. 1995;12(1):49-59.
- [13] Downey DB, Nicolle DA, Fenster A. Three-dimensional orbital ultrasonography. *Can J Ophthalmol*. 1995;30(7):395-8.
- [14] Downey DB, Nicolle DA, Fenster A. Three-dimensional ultrasound of the eye. *Administrative Radiology Journal*. 1995;14:46-50.
- [15] Gilja OH, Thune N, Matre K, Hausken T, Odegaard S, Berstad A. In vitro evaluation of three-dimensional ultrasonography in volume estimation of abdominal organs. *Ultrasound Med Biol*. 1994;20(2):157-65.
- [16] Bax J, Cool D, Gardi L, Knight K, Smith D, Montreuil J, et al. Mechanically assisted 3D ultrasound guided prostate biopsy system. *Med Phys*. 2008;35(12):5397-410.
- [17] Goncalves L, Nien J, Espinoza J, Kusanovic J, Lee W, Swope B, et al. Two-Dimensional (2D) versus three- and four-dimensional (3D/4D) us in obstetrical practice: Does the new technology add anything? *American Journal of Obstetrics and Gynecology*. 2005;193(6):S150-S.
- [18] Peralta CF, Cavoretto P, Csapo B, Falcon O, Nicolaides KH. Lung and heart volumes by three-dimensional ultrasound in normal fetuses at 12-32 weeks' gestation. *Ultrasound Obstet Gynecol*. 2006;27(2):128-33.
- [19] Kurjak A, Miskovic B, Andonotopo W, Stanojevic M, Azumendi G, Vrcic H. How useful is 3D and 4D ultrasound in perinatal medicine? *J Perinat Med*. 2007;35(1):10-27.
- [20] Blake CC, Elliot TL, Slomka PJ, Downey DB, Fenster A. Variability and accuracy of measurements of prostate brachytherapy seed position in vitro using three-dimensional ultrasound: an intra- and inter-observer study. *Med Phys*. 2000;27(12):2788-95.
- [21] Fenster A, Downey DB, Cardinal HN. Three-dimensional ultrasound imaging. *Phys Med Biol*. 2001;46(5):R67-99.
- [22] Downey DB, Fenster A. Vascular imaging with a three-dimensional power Doppler system. *AJR Am J Roentgenol*. 1995;165(3):665-8.
- [23] Picot PA, Rickey DW, Mitchell R, Rankin RN, Fenster A. Three-dimensional colour Doppler imaging. *Ultrasound Med Biol*. 1993;19(2):95-104.
- [24] Pretorius DH, Nelson TR, Jaffe JS. 3-dimensional sonographic analysis based on color flow Doppler and gray scale image data: a preliminary report. *J Ultrasound Med*. 1992;11(5):225-32.
- [25] Downey DB, Fenster A. Three-dimensional power Doppler detection of prostate cancer [letter]. 1995;165(3):741.

- [26] Landry A, Fenster A. Theoretical and experimental quantification of carotid plaque volume measurements made by 3D ultrasound using test phantoms. *Medical Physics*. 2002.
- [27] Landry A, Ainsworth C, Blake C, Spence JD, Fenster A. Manual planimetric measurement of carotid plaque volume using three-dimensional ultrasound imaging. *Medical Physics*. 2007;34(4):1496-505.
- [28] Landry A, Spence JD, Fenster A. Quantification of carotid plaque volume measurements using 3D ultrasound imaging. *Ultrasound Med Biol*. 2005;31(6):751-62.
- [29] Ainsworth CD, Blake CC, Tamayo A, Beletsky V, Fenster A, Spence JD. 3D Ultrasound Measurement of Change in Carotid Plaque Volume; A Tool for Rapid Evaluation of New Therapies. *Stroke*. 2005;35:1904-9.
- [30] Krasinski A, Chiu B, Spence JD, Fenster A, Parraga G. Three-dimensional Ultrasound Quantification of Intensive Statin Treatment of Carotid Atherosclerosis. *Ultrasound in Medicine & Biology*. 2009;35(11):1763-72.
- [31] Bamber JC, Eckersley RJ, Hubregtse P, Bush NL, Bell DS, Crawford DC. Data processing for 3-D ultrasound visualization of tumour anatomy and blood flow. *SPIE*. 1992;1808:651-63.
- [32] Carson PL, Li X, Pallister J, Moskalik A, Rubin JM, Fowlkes JB. Approximate quantification of detected fractional blood volume and perfusion from 3-D color flow and Doppler power signal imaging. 1993 ultrasonics symposium proceedings. Piscataway, NJ: IEEE; 1993. p. 1023-6.
- [33] King DL, King DLJ, Shao MY. Evaluation of in vitro measurement accuracy of a three-dimensional ultrasound scanner. *J Ultrasound Med*. 1991;10(2):77-82.
- [34] Tong S, Downey DB, Cardinal HN, Fenster A. A three-dimensional ultrasound prostate imaging system. *Ultrasound Med Biol*. 1996;22(6):735-46.
- [35] Tong S, Cardinal HN, McLoughlin RF, Downey DB, Fenster A. Intra- and inter-observer variability and reliability of prostate volume measurement via two-dimensional and three-dimensional ultrasound imaging. *Ultrasound Med Biol*. 1998;24(5):673-81.
- [36] Downey DB, Chin JL, Fenster A. Three-dimensional US-guided cryosurgery. *Radiology*. 1995;197(P):539.
- [37] Chin JL, Downey DB, Elliot TL, Tong S, McLean CA, Fortier M, et al. Three dimensional transrectal ultrasound imaging of the prostate: clinical validation. *Can J Urol*. 1999;6(2):720-6.
- [38] Onik GM, Downey DB, Fenster A. Three-dimensional sonographically monitored cryosurgery in a prostate phantom. *J Ultrasound Med*. 1996;15(3):267-70.

- [39] Wei Z, Gardi L, Downey DB, Fenster A. Oblique needle segmentation and tracking for 3D TRUS guided prostate brachytherapy. *Med Phys*. 2005;32(9):2928-41.
- [40] Cool D, Sherebrin S, Izawa J, Chin J, Fenster A. Design and evaluation of a 3D trans-rectal ultrasound prostate biopsy system. *Med Phys*. 2008;35(10):4695-707.
- [41] Treece G, Prager R, Gee A, Berman L. 3D ultrasound measurement of large organ volume. *Med Image Anal*. 2001;5(1):41-54.
- [42] Detmer PR, Bashein G, Hodges T, Beach KW, Filer EP, Burns DH, et al. 3D ultrasonic image feature localization based on magnetic scanhead tracking: in vitro calibration and validation. *Ultrasound Med Biol*. 1994;20(9):923-36.
- [43] Hodges TC, Detmer PR, Burns DH, Beach KW, Strandness DEJ. Ultrasonic three-dimensional reconstruction: in vitro and in vivo volume and area measurement. *Ultrasound Med Biol*. 1994;20(8):719-29.
- [44] Hughes SW, D'Arcy TJ, Maxwell DJ, Chiu W, Milner A, Saunders JE, et al. Volume estimation from multiplanar 2D ultrasound images using a remote electromagnetic position and orientation sensor. *Ultrasound Med Biol*. 1996;22(5):561-72.
- [45] Leotta DF, Detmer PR, Martin RW. Performance of a miniature magnetic position sensor for three-dimensional ultrasound imaging. *Ultrasound Med Biol*. 1997;23(4):597-609.
- [46] Gilja OH, Detmer PR, Jong JM, Leotta DF, Li XN, Beach KW, et al. Intra-gastric distribution and gastric emptying assessed by three-dimensional ultrasonography. *Gastroenterology*. 1997;113(1):38-49.
- [47] Nelson TR, Pretorius DH. Visualization of the fetal thoracic skeleton with three-dimensional sonography: a preliminary report. *AJR Am J Roentgenol*. 1995;164(6):1485-8.
- [48] Pretorius DH, Nelson TR. Prenatal visualization of cranial sutures and fontanelles with three-dimensional ultrasonography. *J Ultrasound Med*. 1994;13(11):871-6.
- [49] Raab FH, Blood EB, Steiner TO, Jones HR. Magnetic position and orientation tracking system. *IEEE Transactions on Aerospace and Electronic Systems*. 1979;AES-15:709-17.
- [50] Riccabona M, Nelson TR, Pretorius DH, Davidson TE. Distance and volume measurement using three-dimensional ultrasonography. *J Ultrasound Med*. 1995;14(12):881-6.
- [51] Hsu PW, Prager RW, Gee AH, Treece GM. Real-time freehand 3D ultrasound calibration. *Ultrasound Med Biol*. 2008;34(2):239-51.
- [52] Jemal A, Bray F, Center MM, Ferlay J, Ward E, Forman D. Global cancer statistics. *CA Cancer J Clin*. 2011;61(2):69-90.

- [53] Jemal A, Siegel R, Xu J, Ward E. Cancer statistics, 2010. *CA Cancer J Clin.* 2010;60(5):277-300.
- [54] Solbiati L, Ierace T, Tonolini M, Cova L. *Ablation of Liver Metastases: Springer, Berlin; 2004. 311 - 21 p.*
- [55] El-Serag HB, Marrero JA, Rudolph L, Reddy KR. Diagnosis and treatment of hepatocellular carcinoma. *Gastroenterology.* 2008;134(6):1752-63.
- [56] Adam A, Mueller P. *Interventional Radiological Treatment of Liver Tumors. Cambridge, UK: Cambridge University Press; 2009.*
- [57] McKay A, Fradette K, Lipschitz J. Long-term outcomes following hepatic resection and radiofrequency ablation of colorectal liver metastases. *HPB Surg.* 2009;2009:346863.
- [58] Seki T. "Microwave Coagulation Therapy for Liver Tumors", *Tumour Ablation, Principle and Practice: Springer; 2004. 218 - 27 p.*
- [59] Haemmerich D, Laeseke PF. Thermal tumour ablation: devices, clinical applications and future directions. *Int J Hyperthermia.* 2005;21(8):755-60.
- [60] Cool DW, Gardi L, Romagnoli C, Saikaly M, Izawa JI, Fenster A. Temporal-based needle segmentation algorithm for transrectal ultrasound prostate biopsy procedures. *Med Phys.* 2010;37(4):1660-73.
- [61] Wang Y, Cardinal HN, Downey DB, Fenster A. Semiautomatic three-dimensional segmentation of the prostate using two-dimensional ultrasound images. *Med Phys.* 2003;30(5):887-97.
- [62] Ding M, Cardinal HN, Fenster A. Automatic needle segmentation in three-dimensional ultrasound images using two orthogonal two-dimensional image projections. *Med Phys.* 2003;30(2):222-34.
- [63] Ding M, Fenster A. A real-time biopsy needle segmentation technique using Hough transform. *Med Phys.* 2003;30(8):2222-33.
- [64] Karnik VV, Fenster A, Bax J, Gardi L, Gyacskov I, Montreuil J, et al. Evaluation of inter-session 3D-TRUS to 3D-TRUS image registration for repeat prostate biopsies. *Med Image Comput Comput Assist Interv.* 2010;13(Pt 2):17-25.
- [65] Rickey DW, Picot PA, Christopher DA, Fenster A. A wall-less vessel phantom for Doppler ultrasound studies. *Ultrasound Med Biol.* 1995;21(9):1163-76.
- [66] McNeal JE, Bostwick DG, Kindrachuk RA, Redwine EA, Freiha FS, Stamey TA. Patterns of progression in prostate cancer. *Lancet.* 1986;1(8472):60-3.
- [67] Garfinkel L, Mushinski M. Cancer incidence, mortality and survival: trends in four leading sites. *Stat Bull Metrop Insur Co.* 1994;75(3):19-27.

- [68] Silverberg E, Boring CC, Squires TS. Cancer statistics, 1990 [see comments]. *CA Cancer J Clin.* 1990;40:9-26.
- [69] Abbas F, Scardino PT. The natural history of clinical prostate carcinoma [editorial; comment]. *Cancer.* 1997;80(5):827-33.
- [70] Shinohara K, Scardino PT, Carter SS, Wheeler TM. Pathologic basis of the sonographic appearance of the normal and malignant prostate. *Urol Clin North Am.* 1989;16(4):675-91.
- [71] Terris MK, McNeal JE, Stamey TA. Estimation of prostate cancer volume by transrectal ultrasound imaging. *J Urol.* 1992;147(3 Pt 2):855-7.
- [72] Rifkin MD. Ultrasound of the prostate-Imaging in the diagnosis and therapy of prostatic disease. 2 ed. Ryan JD, Patterson D, DiFrancesco R, editors. Philadelphia, New York: Lippincott-Raven Publishers; 1997.
- [73] Djavan B, Zlotta AR, Ekane S, Remzi M, Kramer G, Roumeguere T, et al. Is one set of sextant biopsies enough to rule out prostate Cancer? Influence of transition and total prostate volumes on prostate cancer yield. *Eur Urol.* 2000;38(2):218-24.
- [74] Djavan B, Remzi M, Schulman CC, Marberger M, Zlotta AR. Repeat prostate biopsy: who, how and when?. a review. *Eur Urol.* 2002;42(2):93-103.
- [75] Matlaga BR, Eskew LA, McCullough DL. Prostate biopsy: indications and technique. *J Urol.* 2003;169(1):12-9.
- [76] Presti JC, Jr., O'Dowd GJ, Miller MC, Mattu R, Veltri RW. Extended peripheral zone biopsy schemes increase cancer detection rates and minimize variance in prostate specific antigen and age related cancer rates: results of a community multi-practice study. *J Urol.* 2003;169(1):125-9.
- [77] Jemal A, Thomas A, Murray T, Thun M. Cancer statistics, 2002. *CA Cancer J Clin.* 2002;52(1):23-47.
- [78] Nelson WG, De Marzo AM, Isaacs WB. Prostate cancer. *N Engl J Med.* 2003;349(4):366-81.
- [79] Park SJ, Miyake H, Hara I, Eto H. Predictors of prostate cancer on repeat transrectal ultrasound-guided systematic prostate biopsy. *Int J Urol.* 2003;10(2):68-71.
- [80] Iczkowski KA, Chen HM, Yang XJ, Beach RA. Prostate cancer diagnosed after initial biopsy with atypical small acinar proliferation suspicious for malignancy is similar to cancer found on initial biopsy. *Urology.* 2002;60(5):851-4.
- [81] Thorson P, Humphrey PA. Minimal adenocarcinoma in prostate needle biopsy tissue. *Am J Clin Pathol.* 2000;114(6):896-909.

- [82] San Francisco I, DeWolf W, Rosen S, Upton M, Olumi A. Extended prostate needle biopsy improves concordance of Gleason grading between prostate needle biopsy and radical prostatectomy. *Urology*. 2003;169:136-40.
- [83] Futterer JJ, Heijmink SW, Scheenen TW, Veltman J, Huisman HJ, Vos P, et al. Prostate cancer localization with dynamic contrast-enhanced MR imaging and proton MR spectroscopic imaging. *Radiology*. 2006;241(2):449-58.
- [84] Hricak H, Choyke PL, Eberhardt SC, Leibel SA, Scardino PT. Imaging prostate cancer: a multidisciplinary perspective. *Radiology*. 2007;243(1):28-53.
- [85] Manenti G, Carlini M, Mancino S, Colangelo V, Di Roma M, Squillaci E, et al. Diffusion tensor magnetic resonance imaging of prostate cancer. *Invest Radiol*. 2007;42(6):412-9.
- [86] Heijmink SW, Futterer JJ, Hambroek T, Takahashi S, Scheenen TW, Huisman HJ, et al. Prostate cancer: body-array versus endorectal coil MR imaging at 3 T--comparison of image quality, localization, and staging performance. *Radiology*. 2007;244(1):184-95.
- [87] Morgan VA, Kyriazi S, Ashley SE, DeSouza NM. Evaluation of the potential of diffusion-weighted imaging in prostate cancer detection. *Acta Radiol*. 2007;48(6):695-703.
- [88] Farsad M, Schiavina R, Castellucci P, Nanni C, Corti B, Martorana G, et al. Detection and localization of prostate cancer: correlation of (11)C-choline PET/CT with histopathologic step-section analysis. *J Nucl Med*. 2005;46(10):1642-9.
- [89] Martorana G, Schiavina R, Corti B, Farsad M, Salizzoni E, Brunocilla E, et al. 11C-choline positron emission tomography/computerized tomography for tumor localization of primary prostate cancer in comparison with 12-core biopsy. *J Urol*. 2006;176(3):954-60; discussion 60.
- [90] Schoder H, Gonen M. Screening for cancer with PET and PET/CT: potential and limitations. *J Nucl Med*. 2007;48 Suppl 1:4S-18S.
- [91] Fenster A, Downey DB, Cardinal HN. Topical Review: Three-dimensional ultrasound imaging. *Phys Med Biol*. 2001;46(5):R67-99.
- [92] Ladak HM, Mao F, Wang Y, Downey DB, Steinman DA, Fenster A. Prostate boundary segmentation from 2D ultrasound images. *Med Phys*. 2000;27(8):1777-88.
- [93] Hu N, Downey DB, Fenster A, Ladak HM. Prostate boundary segmentation from 3D ultrasound images. *Med Phys*. 2003;30(7):1648-59.
- [94] Cool D, Downey D, Izawa J, Chin J, Fenster A. 3D prostate model formation from non-parallel 2D ultrasound biopsy images. *Med Image Anal*. 2006;10(6):875-87.

